MID-AMERICA TRANSPORTATION CENTER

Report # MATC-UI: 141-3

Final Report
WBS: 25-1121-0005-141-3

Development of New Design Guidelines for Protection Against Erosion at Bridge Abutments, Phase III

George Constantinescu, PhD, PI
Professor
Department of Civil and Environmental Engineering
University of Iowa

Hao Wu
Graduate Research Assistant

2020

A Cooperative Research Project sponsored by
U.S. Department of Transportation- Office of the Assistant Secretary for Research and Technology

Development of New Design Guidelines for Protection against Erosion at Bridge Abutments Phase III

George Constantinescu, Ph.D., PI
Professor
Department of Civil and Environmental Engineering
The University of Iowa

Hao Wu
Graduate Research Assistant
Department of Civil and Environmental Engineering
The University of Iowa

A Report on Research Sponsored by

Mid-America Transportation Center

University of Nebraska–Lincoln

December 2020

Technical Report Documentation Page

1. Report No. 25-1121-0005-141-3	2. Government Accession No.	3. Recipient's Catalog No.
4. Title and Subtitle Development of New Design Guidelines for Protection against Erosion at Bridge Abutments, Phase III		5. Report Date December 2020 6. Performing Organization Code
7. Author(s) George Constantinescu, Ph.D., PI ORCID: https://orcid.org/0000-0001-7060-8378 Hao Wu		8. Performing Organization Report No. 25-1121-0005-141-3
9. Performing Organization Name and Address Department of Civil and Environmental Engineering The University of Iowa Iowa City, IA 52242		10. Work Unit No. 11. Contract or Grant No. 69A3551747107
12. Sponsoring Agency Name and Address Mid-America Transportation Center 2200 Vine St. PO Box 830851 Lincoln, NE 68583-0851		13. Type of Report and Period Covered Final Report Sept 2019 - Aug 2020 14. Sponsoring Agency Code MATC TRB RiP No. 91994-46
15. Supplementary Notes Conducted in cooperation with the U.S. Department of Transportation, Federal Highway Administration.		

16. Abstract

Maintaining road operations requires reliable and safe transportation infrastructure design, in particular for bridges that need to remain operational during floods and other extreme weather events. A numerically based investigation is carried out to determine the minimum median diameter of the riprap stone needed to avoid shear failure inside the riprap apron used to protect spill-trough abutments against erosion. The numerically-based approach was validated for wing-wall abutments placed in a straight channel based on data from laboratory experiments. This Year 3 report discusses results of several series of Reynolds-Averaged Navier-Stokes (RANS) simulations conducted with varying floodplain width, B_f, ratio between the abutment length and the floodplain width, L_a/B_f, mean diameter of the riprap stone, D_{50}, and channel radius of curvature, R, to estimate the maximum Froude number, Fr, at which riprap stones in aprons placed at the base of spill-through abutments will resist shear failure. Analysis of the data shows that existing design formulas are not sufficiently conservative for some of the test cases conducted with straight channels. A two-parameter design formula for riprap size selection in aprons protecting abutments against local scour is proposed for spill-through abutments placed in straight compound channels. This formula will be extended for abutments placed in a curved channel.

17. Key Words Bridges, Bridge scour, Bridge abutment, Local Scour, Rip-rap protection against scour	18. Distribution Statement No restrictions. This document is available through the National Technical Information Service, Springfield, VA 22161.

19. Security Classif. (of this report) Unclassified	20. Security Classif. (of this page) Unclassified	21. No. of Pages 41	22. Price

Form DOT F 1700.7 (8-72) Reproduction of completed page authorized

Table of Contents

List of Figures

List of Tables

Acknowledgments

We would like to thank Prof. Bruce Melville form University of Auckland, New Zeeland for providing additional information on his experiments carried for wing-wall abutments.

Disclaimer

The contents of this report reflect the views of the authors, who are responsible for the facts and the accuracy of the information presented herein. This document is disseminated in the interest of information exchange. The report is funded, partially or entirely, by a grant from the U.S. Department of Transportation's University Transportation Centers Program. However, the U.S. Government assumes no liability for the contents or use thereof.

Abstract

Severe floods in the United States Midwest have caused major erosion at bridge abutments despite their protection design measures following existing guidelines (e.g., HEC 23, 2001 and following updates through 2009). At high-flow conditions, erosion occurs not only inside the main channel but also over its floodplains especially in the region of flow contraction induced by the presence of obstructions such as bridge piers, bridge abutments and the attached embankments (e.g., see Sturm and Janjua, 1994, Sumer and Fredsoe, 2002). Severe scour can endanger the stability of the embankment and induce scour beneath the foundations of the abutments. Placing riprap stone around the base of each abutment and over its erodible faces is the most common way to protect abutments against erosion (e.g., see NCHRP Projects 24-18, 24-19, 24-20). One likely possibility for the severe local scour at abutments is that existing design formulas to calculate the minimum size of the riprap stone used for protection of wing-wall and spill-through abutments (e.g., Lagasse et al., 2001; Pagan-Ortiz, 1991) are based on an oversimplified approach. Moreover, such formulas do not account for complexities associated with these structures being placed in natural streams where, for instance, bank curvature effects may be important. The coefficients in these formulas were determined based on a limited series of laboratory experiments conducted for a relatively narrow range of relevant geometrical and flow parameters that influence the capacity of the flow to induce erosion at such bridge sites.

This project aims to improve the performance and range of applicability of riprap design formulas used for erosion protection at wing-wall and spill-through abutments. The mean flow fields and the bed shear stress distributions are obtained from fully three-dimensional, non-hydrostatic RANS simulations. These data are then used to estimate the maximum bed shear stress over the riprap apron, the shear-failure entrainment threshold for the riprap stone and the

other variables in the design formulas recommended in HEC 23. The approach was validated for the case of wing-wall abutments placed in a straight channel based on data from laboratory experiments. The present Year 3 report describes how relative abutment length, floodplain width, and channel curvature affect the maximum bed shear stress over the region protected by riprap for spill-through abutments placed over the floodplains of compound channels. Using data obtained from numerical experiments, a new, two-parameter design formula for riprap sizing at spill-through abutments placed in a straight channel is proposed.

Chapter 1 Introduction

1.1 Motivation and Proposed Approach

Reliable and safe transportation infrastructure design for flooding events is a main task for state and federal agencies in charge of maintaining our road operational. The US Midwest has experienced increasingly catastrophic flood events over the last few decades. Severe erosion problems were reported at many bridge sites, especially for abutments and embankments of smaller-size bridges. Severe scour can endanger the stability of the embankment and induce scour beneath the foundations of the abutments. In extreme cases, this may lead to bridge failure which results in interrupting the traffic and, in some cases, to loss of human life. Two of the most encountered types of abutments used at bridges are spill-through and wing-wall abutments.

Considerable progress has been made over the two decades in understanding the mechanisms of local scour at abutments and in developing effective bridge-scour countermeasures to protect these structures against severe erosion (e.g., Sumer and Fredsoe, 2002, Melville and Coleman, 2000, Dey and Barbhuiya, 2005, Kothyari at al., 2007, Sturm et al., 2011, Ettema et al., 2011, 2015, 2017, Koken and Constantinescu, 2014, Hong and Abid, 2019). Placing riprap stone around the base of a bridge abutment, where the highest stresses generally occur, and over its erodible faces is one of the most common ways to protect abutments against erosion (Brown and Clyde, 1989, Melville and Coleman, 2000). The riprap stone provides an armor layer protection to the finer sediments present near the bed surface. When placed near the base of an abutment, the main effect of the apron is to modify the geometry of the scour hole such that the maximum scour depth is reduced and the locations of large scour move away from the base/toe of the abutment.

The riprap stone forming the abutment apron may be subjected to several modes of failure including shear failure, winnowing failure, and edge failure (Melville et al., 2007). In general, the minimum size of the riprap stone in design equations is determined such that shear and edge failure are avoided (Chiew, 1995, Melville et al., 2007, Barkdoll et al., 2007). Shear failure occurs where the individual riprap stones are not large enough to resist entrainment by the flow. In general, design guidelines for bridge piers and abutments (e.g., Hoffmans and Verheij, 1997, Lagasse et al., 2001, Sumer and Fredsoe, 2002, Melville and Coleman, 2000, Melville et al., 2006a, 2006b, Cardoso et al., 2010) are mostly based on laboratory experiments (flume studies) conducted for a limited range of flow conditions (e.g., straight channels, limited width of the floodplain). None of these design formulas can be used for cases when bank curvature effects are important or pressure scour effects due to bridge deck submergence are present. Another general characteristic of most existing design formulas for bridge abutments is the minimum size of the median diameter of the riprap stone, D_{50}, in these formulas is only a function of the Froude number defined with the mean velocity in the contracted region containing the abutment and the flow depth. The effects of important geometrical parameters that affect the flow and its capacity to entrain sediment near bridge abutments (e.g., the floodplain width and the relative abutment length in the case of spill-through abutments) are not accounted for in these formulas. Thus, there is a need to improve these guidelines and propose modified formulas or methodologies that can provide effective protection against erosion for a larger range of flow and geometrical conditions at these two types of abutments.

One possible alternative to flume studies is to use numerical simulations to estimate the boundary shear stress over the channel bed, including over the regions protected by rock riprap. Fully 3-D, non-hydrostatic Reynolds-Averaged Navier-Stokes (RANS) models using two-

equation turbulence closures are generally quite successful to predict flow and bed shear stress distributions in natural channels containing hydraulic structures (Roulund et al., 2005). Such models can account for the effect of the bed roughness on the flow and turbulence inside the channel (Zeng et al., 2008). If such a numerical approach is adopted, a series of 3-D simulations may be used to determine whether the riprap stone inside the apron will fail or not. For a given channel and abutment geometry, incoming flow discharge and flow depth, the predicted maximum shear stress over the riprap region is compared with the critical value for riprap failure to determine if the riprap stone will be entrained or not into the water column. To estimate the critical Froude number corresponding to the shear-failure entrainment threshold for the riprap stone, the discharge is then varied until the maximum bed shear stress over the riprap region is equal to the critical value.

1.2 Prior Main Results and Findings

Figure 1.1 shows the general layout of the computational domain and the main geometrical variables (B_f=floodplain width, L_a=abutment length, y_m=flow depth over main channel, y_f=flow depth over the floodplains), as well as the position of the riprap apron. Outside of the riprap apron, the flat bed was covered with sand with d_{50}=0.82 mm. The inlet discharge was varied until the maximum value of the bed friction velocity over the riprap layer was $0.35u_{*cr}$, where u_{*cr} is obtained from the Shields diagram for a given mean diameter of the riprap stone, D_{50}. Following Melville and Coleman (2000), this value was used to determine the riprap shear failure entrainment threshold. The Froude number, Fr, was calculated using the mean velocity in the section containing the abutment.

The main research activity conducted during Year 1 was the validation of the method using the experimental data of Melville et al. (2007) for wing-wall abutments placed in a straight

channel (fig. 1.1a). Simulations were conducted with flow only inside the main channel (y_m=0.1 m) and with flow over the floodplain (y_m=0.17 m, y_f=0.07 m) for B_f=0.4 m, 1.4 m, and 20 m and for 20 mm<D_{50}<61 mm. Five of the simulated test cases of the wing-wall abutment corresponded to those in the experiments of Melville et al. (2007). Figure 1.2 shows that for each of the five series of experiments, the numerically predicted shear failure entrainment threshold was situated in between the limiting experiments where no shear failure and, respectively, shear failure were observed.

During Year 2, a comprehensive parametric study was conducted for straight and curved channels containing wing-wall abutments at their two banks. Simulations were conducted for normal flow conditions (y_m=0.1 m) and with flow over the floodplains (y_m=0.17 m, y_f=0.07 m) and with varying riprap diameter (D_{50}=20 mm, 28 mm, 40 mm and 60 mm), floodplain width (B_f/W=0, 0.2 and 0.7) and channel radius of curvature (R/W=∞, 20, 10 and 1), where W=2 m is the width of the main channel. Using these data, the performance of existing design formulas (Pagan-Ortiz,1991 and Lagasse et al., 2001) for riprap protection at bridges containing wing-wall abutments was checked for a wide range of conditions, outside of the range used to calibrate these formulas. A main finding was the two design formulas are not conservative enough for straight channels with a large floodplain width (Case III in Figure 1.3a). The design formulas were also found not to be conservative enough for cases where the abutments were placed in channels with a relatively high curvature (R/W<20).

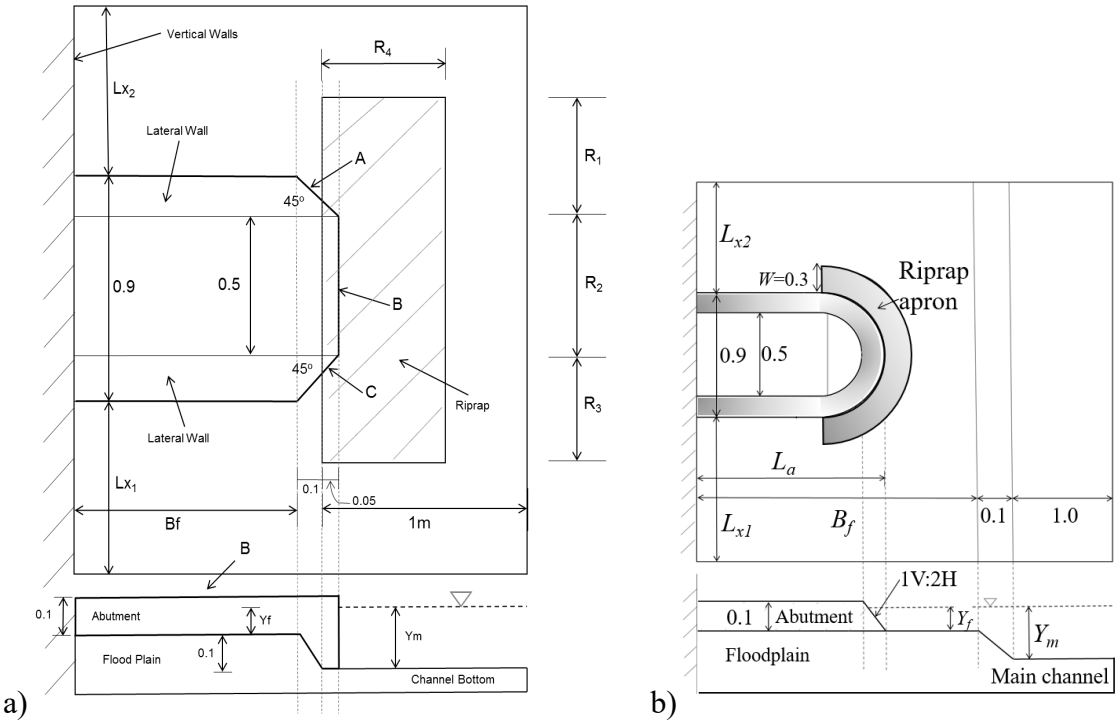

Figure 1.1 Sketch showing general layout of the preliminary numerical simulations performed for a wing-wall abutment (left) and for a spill-through abutment (right) placed on the floodplain of a straight channel. Dimensions are in meters. The wing-wall abutment geometrical set up corresponds to that used in the laboratory experiments of Melville et al. (2007). Reproduced from Wu et al. (2020a) and Wu et al., (2020b).

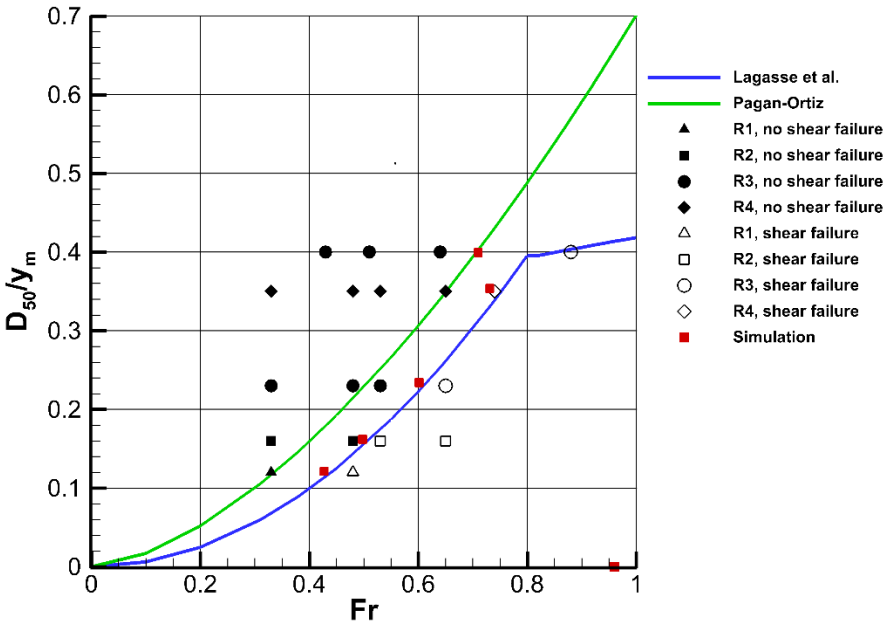

Figure 1.2 Comparison of numerical results with Lagasse et al. (2001) and Pagan-Ortiz (1991) equations and the experimental data of Melville et al. (2007) for a wing-wall abutment in a straight channel. Simulation data always show predicted conditions for threshold of riprap stone entrainment by shear failure. Experimental data only show if shear failure occurred (open symbols or not (solid symbols) in the corresponding experiments. Reproduced from Wu et al. (2020a).

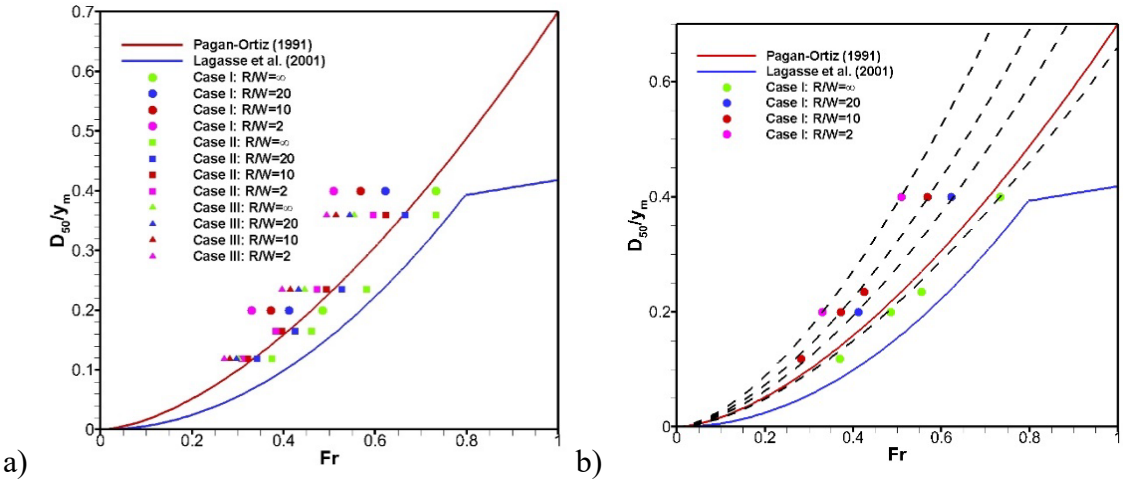

Figure 1.3 Comparison of numerical results with Lagasse et al. (2001) and Pagan-Ortiz (1991) equations for wing-wall abutments placed in straight and curved channels. The floodplain width is $B_f/W=0$ for Case I, $B_f/W=0.2$ for Case II and $B_f/W=0.7$ for Case III. Simulation data show predicted conditions for treshold of riprap entrainment by shear failure. The dashed lines in frame b show the new design formula predictions for Case I simulations. Partially reproduced from Wu et al. (2020a).

The other main contribution of Year 2 was to propose a new design formula that retains the same functional relationship as that of Pagan-Ortiz (1991) and Lagasse et al. (2001) formulas:

$$D_{50}/y=(K_s/(S_s-1))^{0.5\alpha} *Fr^{\alpha}=C^{0.5\alpha}*Fr^{\alpha} \quad (1.1)$$

where K_s is the shape factor, S_s=2.65 is the specific gravity of the riprap stone, $C=K_s/(S_s-1)$ is a model coefficient and Fr is defined with the mean velocity in the section containing the abutments, V, and a characteristic length scale, y. For wing-wall abutments, $y=y_m$. Using this formulation, C=0.645 and α =1.62 for Pagan-Ortiz (1991) formula and C=0.618 and α =2.0 for Lagasse et al. (2001) formula (Fr<0.8). In the new design formula for wing-wall abutments, C and α are a function of the main nondimensional geometrical parameters (e.g., B_f/W, R/W). More details are given in Wu et al. (2020a). One major finding was that α is not a function of the channel curvature, R/W, but increases monotonically with increasing B_f/W. The predicted range for α ($1.62<\alpha<1.84$) was in between the values used by the Pagan-Ortiz (1991) formula (α=1.62) and Lagasse et al. (2001) formula (α=2).

1.3 Objectives

The main research objectives for Year 3 are to:

1. Perform a comprehensive set of numerical experiments to determine the shear-failure entrainment threshold for the riprap apron protecting spill-through abutments positioned on the floodplains of straight and curved channels over a relevant range of the (nondimensional) radius of curvature of the channel, floodplain width and relative abutment length;

2. Test performance of main design formulas recommended by HEC 23 (Lagasse et al., 2001; Pagan-Ortiz, 1991) to estimate the minimum median diameter of the riprap stone used for protection against erosion for spill-through abutments placed in straight compound channels; and
3. Propose a two-parameter design formula that can be applied for riprap sizing at spill-through abutments placed in straight channels that incorporates the effects of the nondimensional floodplain width and relative abutment length.

1.4 Justification of Research Approach

Understanding and being able to quantitatively describe how the hydrodynamics of the stream flow field (velocity magnitude and bed shear stress distributions around the bridge site) changes with increasing stage and discharge as a result of a flood is critical to be able to propose effective measures to protect bridge abutments and piers against erosion. The National cooperative Highway Research Program Report 587 (NCHRP Report 587) used in the development of HEC 23 (2001, 2009) states the following:

> Selection of countermeasures to protect bridges from scour requires estimates of velocity distributions in the bridge opening. Estimates of the peak velocity in what is typically a highly non-uniform flow distribution near the tip of the abutment is necessary to determine whether countermeasures are necessary and, if so, to determine the type, size, and extent of countermeasures to protect bridge abutments from scour. Laboratory physical models have been developed to determine the size, type, and location of protection for a relatively small range of flow conditions at bridges; however, the laboratory models represent very simplistic geometric conditions. Effective transfer of laboratory model results to the complex hydrodynamic conditions of real bridge sites requires that flow velocity be predicted in the vicinity of bridge abutments using numerical models.

The report also comments on the limitations of the two-dimensional (2-D) depth-averaged modeling approach which was used in past studies to provide more accurate estimations of the variables in the design formulas used to protect against erosion. The main

limitations of the 2-D approach are due to the hydrostatic pressure assumption and simplified turbulence modeling. Moreover, the region of maximum velocity amplification near the abutment toe is generally located in a region of high flow curvature where 2-D numerical models are not very accurate.

The present study uses fully three-dimensional (3-D), non-hydrostatic, RANS simulations performed on fine meshes to obtain the 3-D mean velocity flow field. This allows direct estimation of the mean boundary shear stress over the whole bed region, including over the riprap apron.

Given the detailed information on the flow fields, turbulence and their effects on the bed shear stress distributions available from such 3-D simulations, the proposed approach can lead to extension of the range of geometrical and flow configurations for which design formulas can be applied (e.g., abutments placed inside or immediately downstream of curved channels, high flow conditions that lead to the bridge deck becoming submerged). For such cases, laboratory experiments are very expensive and the range of geometrical (e.g., channel aspect ratio, width of the floodplain) and flow parameters in these experiments are even more limited compared to the canonical case of an abutment placed in a straight channel. The numerically based approach adopted in the present study does not face these limitations.

Chapter 2 Numerical Method

STAR-CCM+ is a state-of-the-art commercial code developed by CD-Adapco which solves the fully 3-D non-hydrostatic Navier-Stokes equations together with the turbulence model equations. The solver uses the finite-volume method to integrate the governing equations and allows the use of unstructured meshes. The RANS turbulence model provides the value of the eddy viscosity. The governing continuity and momentum equations are:

$$\frac{\partial U_i}{\partial x_i} = 0 \tag{2.1}$$

$$\frac{\partial U_i}{\partial t} + \frac{\partial (U_i U_k)}{\partial x_k} = -\frac{1}{\rho}\frac{\partial P}{\partial x_i} + \frac{1}{\rho}\frac{\partial}{\partial x_k}\left[(\mu + \mu_t)\left(\frac{\partial U_i}{\partial x_k} + \frac{\partial U_k}{\partial x_i}\right)\right] - g\hat{k} \tag{2.2}$$

where

U_i = Reynolds Averaged velocity component along the i direction

ρ = fluid density

μ = molecular dynamic viscosity

μ_t = eddy viscosity calculated from the RANS turbulence model

P = pressure

g = gravitational acceleration

$\hat{k}$ = unit normal vector along the vertical direction

The discretised Navier-Stokes equations are solved using a fractional-step algorithm. The advective terms are discretised using the second-order accurate upwind scheme, while the transient term discretization in time is second-order accurate based on an implicit representation.

The diffusive terms and the pressure gradient terms are discretised using the second-order accurate central scheme. The pressure-coupling is achieved using the SIMPLE algorithm. In the SIMPLE algorithm, the momentum equations without the pressure gradient term are advanced in time and an intermediate velocity is obtained which does not satisfy the continuity equation. A pressure-correction algorithm is then employed to modify the pressure field such that mass conservation is achieved.

Several two-equation turbulence models available in STAR-CCM+ were initially considered. The k-w SST model performed more accurately for channel flow simulations with a large value of the relative bed roughness, leading to its use in the simulations reported in this paper. STAR-CCM+ with the k-w SST turbulence model was widely used and validated for predictions of flow in channels containing hydraulic structures (Cheng et al., 2018), including for cases when an unsteady flood wave advanced in a channel with natural bathymetry (Cheng et al., 2018 and Horna-Munoz and Constantinescu, 2018, 2020).

No-slip boundary conditions were specified at all wall boundaries. The bed shear was calculated using the law of the wall for rough surfaces. At the rough-wall boundaries, the specified value of the surface roughness k_s was different over the riprap region ($k_s=D_{50}$) and over the rest of the channel bed that was assumed to be covered by a layer of sand ($k_s=d_{50}$). The outlet was specified as a pressure outlet boundary. Given the low value of the channel Froude number, the free surface was treated as a slip (symmetry) boundary on which the vertical velocity was set equal to zero. Preliminary straight and curved channel flow, steady RANS simulations with periodic boundary conditions in the streamwise direction were performed to obtain a fully developed channel flow solution to be used to specify the inlet boundary condition in the corresponding simulations of flow in compound channels containing an abutment on each

floodplain. The cross section of the channel used in the preliminary simulations was identical to the inlet section of the computational domain in the simulations where abutments were present. The 2-D distributions of the velocity and the turbulence variables from the periodic simulations were specified at the inlet of the domain containing the abutments. All simulations were performed in domains containing abutments at both sides of the channel. This is needed because in the case of curved channels the flow field is not symmetrical with respect to the axis of the main channel.

The compound channel cross section is symmetrical with respect to the centerline of the main channel and the spill-through abutments placed over the two floodplains are identical. STAR-CCM+ contains a very powerful meshing capability in which an initial geometry can be imported and smoothed in such a way to improve computational efficiency without loss of critical information. Once the geometry has been processed, a volume mesh is created with the desired meshing model to obtain a high-quality mesh. The grid generator allows the use of various controls and the generation of fine meshes in different parts of the domain where flow resolution needs to be higher (e.g., near the solid surfaces to resolve the attached boundary layers), which is essential to generate a high quality mesh. One of the main advantages of the grid generator in STAR-CCM+ is that it allows automatic grid refinement in critical regions situated around the abutments with a smooth transition to regions where the mesh is coarser.

Chapter 3 Spill-Wall Abutments Placed in Straight and Curved Channels

Spill-through abutments are usually set back on floodplains (fig. 1.1b). At high-flow conditions, the flow over the floodplain contracts as it enters the bridge crossing region, which generally leads to erosion developing around the toe of the abutments. For such flow conditions, the maximum scour depth at spill-through abutments that are set back from the channel's banks can attain several times the incoming flow depth over the floodplain. To reduce erosion developing at the toe of such abutments, a riprap collar is placed around each abutment's toe.

Many bridges are built inside, or immediately downstream, of regions where bank curvature is important (e.g., the ratio between the radius of curvature and the channel width is larger than 20). For such cases, the approaching velocity field around the abutment is quite different compared to the case of a straight channel, with the streamwise velocity being larger close to the abutment situated at the outer bank of the curved channel, at least for small to moderate channel curvatures. High-flow conditions, where the floodplain becomes submerged, add to the flow complexity for cases when abutments are situated inside or close to regions where the channel is not straight.

The geometry of the spill-through abutments (fig. 1.1b) is very similar to that used in the laboratory experiments of Melville et al. (2006b), while the compound channel geometry is identical to that used in the corresponding simulations conducted with wing-wall abutments. The abutment has a trapezoidal cross section. The slope of the sidewalls is 1V:2H and the bottom width of the abutment is 0.9 m. The width of the riprap apron protecting each abutment is W=0.3 m. The width of the main channel is B_m=2 m. The width of the transition region between the main channel and its floodplain is 0.1 m. The difference between the bed elevation over the

floodplain and over the main channel is 0.1 m. In the simulations conducted with $L_a=B_f$, the riprap apron is partially situated inside the main channel.

For simplicity, in the test cases performed with spill-through abutments the channel radius of curvature is assumed to be constant and the nondimensional ratio of curvature is defined as the ratio between the radius of curvature of the main channel centerline, R, and the width of the main channel, B_m.

3.1 Description of Test Cases and RANS Solutions

Simulations in channels containing spill-through abutments at their sides were performed with different values of the riprap mean diameter, D_{50}, and for a flow depth (y_m=0.17 m, y_f=0.07 m) corresponding to flood conditions. Figure 3.1 shows the computational domain used in one of the test cases in which the channel was straight. In the curved channel simulations, the streamwise length of the computational domain between the abutments and the inlet/outlet sections was varied with respect to the straight channel simulations to insure the regions where the flow patterns were affected by the presence of the two abutments did not reach the inlet and outlet boundaries. More details are given in Wu et al. (2020b), on which the discussion below is based.

The width of the main channel was kept constant, B_m=2 m. The difference between the bed elevation over the floodplain and over the main channel was 0.1 m. This is also the length scale (H_{ref}=0.1 m) used to nondimensionalize the different variables. The velocity scale was V=0.4 m/s. The Reynolds number defined with the velocity and length scale was Re=40,000. For flood conditions, the relationship between the flow depth over the floodplain, y_f, and the main channel depth is $y_f=y_m$-0.1 m. The mean diameter of the sand covering the channel bed outside of the regions protected by riprap stone is d_{50}=0.82 mm.

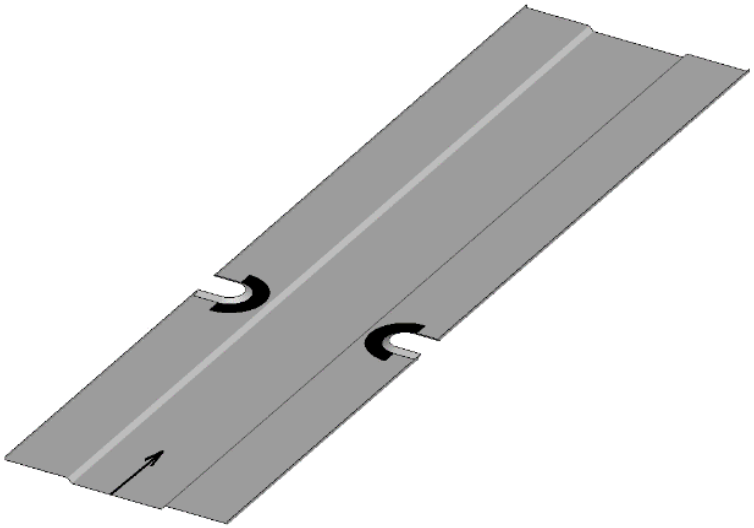

Figure 3.1 Sketch showing computational domain in the straight channel cases containing a spill-through abutment at each bank. Also shown is the riprap apron around the toe of each abutment.

Several series of simulations were conducted for four values of the floodplain width B_f/H_{ref}=5, 10, 14 and 20. These series of simulations conducted with a constant value of B_f/H_{ref} are denoted Case I, Case II, Case III and Case IV in table 3.1, respectively. For each case, simulations were conducted with two different values of the riprap median diameter, D_{50}/H_{ref}=0.2 and 0.4 and three values of the radius of curvature measured along the centerline of the main channel, $R/H_{ref}=\infty$ (straight channel) and R/H_{ref}=400 and 200 (R/B_m=20 and 10). The relative abutment length range was $0.35<L_a/B_f\leq 1$ (table 3.1). The nondimensional values of the critical bed friction velocity for riprap shear failure were $u_{\tau c}/V$=0.12 and 0.175 for D_{50}/H_{ref}=0.2 and 0.4, respectively. The mean streamwise velocity in the cross section containing the two abutments was used to calculate the Froude number, Fr. For each test case, the inlet discharge was varied in a series of simulations until two of the simulations predicted a maximum bed shear stress over the riprap apron slightly larger and, respectively, slightly smaller than the critical

value for riprap shear failure determined following the procedure outlined in Melville et al. (2007).

Table 3.1 Matrix of test cases considered for compound channels containing a spill-through abutment over each floodplain. Reproduced from Wu et al. (2020b).

Test Case	B_f/H_{ref}	B_f/B_m	L_a/H_{ref}	L_a/B_f	R/H_{ref}	R/B_m	D_{50}/H_{ref}
Case I	5	0.25	5	1.0	∞	∞	0.2, 0.4
					400	20	0.2, 0.4
					200	10	0.2, 0.4
Case II	10	0.5	5	0.5	∞	∞	0.2, 0.4
					400	20	0.2, 0.4
					200	10	0.2, 0.4
			7	0.7	∞	∞	0.2, 0.4
					400	20	0.2, 0.4
					200	10	0.2, 0.4
			10	1.0	∞	∞	0.2, 0.4
					400	20	0.2, 0.4
					200	10	0.2, 0.4
Case III	14	0.7	4.9	0.35	∞	∞	0.2, 0.4
					400	20	0.2, 0.4
					200	10	0.2, 0.4
			7	0.5	∞	∞	0.2, 0.4
					400	20	0.2, 0.4
					200	10	0.2, 0.4
			9.8	0.7	∞	∞	0.2, 0.4
					400	20	0.2, 0.4
					200	10	0.2, 0.4
			14	1.0	∞	∞	0.2, 0.4
					400	20	0.2, 0.4
					200	10	0.2, 0.4
					∞	∞	0.2, 0.4

Test Case	B_f/H_{ref}	B_f/B_m	L_a/H_{ref}	L_a/B_f	R/H_{ref}	R/B_m	D_{50}/H_{ref}
Case IV	20	1.0	7	0.35	400	20	0.2, 0.4
					200	10	0.2, 0.4
			10	0.5	∞	∞	0.2, 0.4
					400	20	0.2, 0.4
					200	10	0.2, 0.4
			14	0.7	∞	∞	0.2, 0.4
					400	20	0.2, 0.4
					200	10	0.2, 0.4

Figure 3.2 shows a view of the computational mesh near one of the abutments. For most simulations, the total number of computational cells was in between five and ten million, where the larger number corresponded to the simulations conducted with a larger floodplain width. The mesh density was increased near the two abutments and near all the solid surfaces to resolve the attached boundary layers. An unstructured mesh was used near the abutments and a structured mesh was used away from them. The average size of the grid cells was gradually increased away from the abutments and the no-slip surfaces, which is essential to guarantee a high-quality mesh. Preliminary simulations were conducted to ensure the steady RANS solutions are grid independent in terms of the flow patterns, the sizes of the recirculation regions near the free surface and the bed-shear stress distributions.

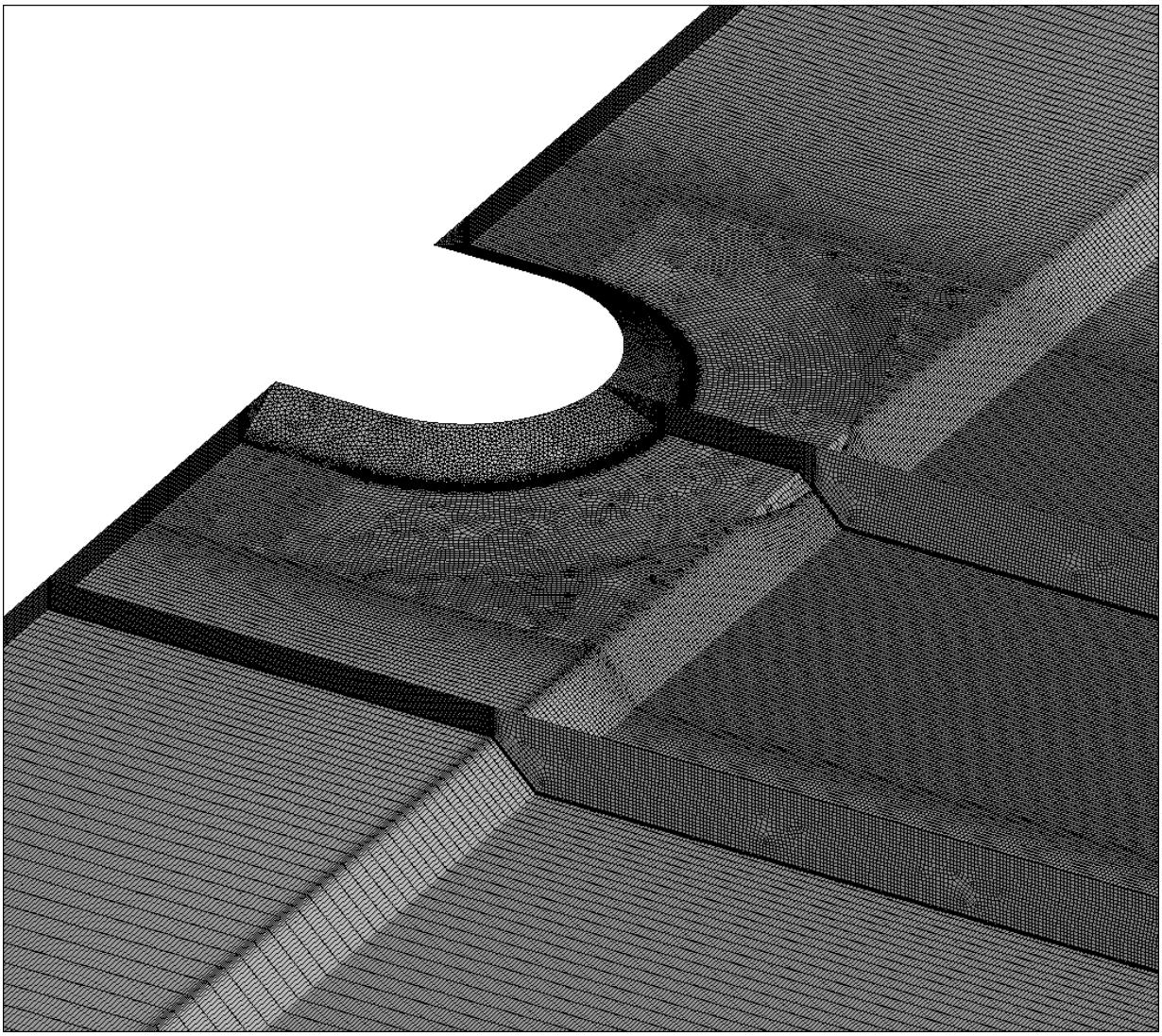

Figure 3.2 Computational mesh around one of the spill-through abutments for a simulation performed in a straight channel with $B_f/H_{ref}=10$ and $L_a/B_f=0.7$. The figure shows the 2-D mesh on the channel surfaces, on the abutment's boundaries and in two cross sections.

Figure 3.3 shows the distributions of the horizontal velocity magnitude at the free surface and bed friction velocity next to one of the spill through abutments for a case where the abutment length is smaller than the floodplain width ($L_a/B_f<1$). One important observation is, opposed to what was observed for wing-wall abutments, the region of highest bed friction velocity is not situated exactly beneath the region of highest velocity magnitude in regions situated away from

the bed. For cases with $L_a/B_f<1$ the largest velocity amplification occurs near the transition region between the floodplain and the main channel. This is expected because the flow accelerates in the contracted region containing the two abutments and, consistent with Manning's equation, the mean streamwise velocity is proportional to the local flow depth. Still, a region of relatively high velocities is recorded near the toe of the abutment, slightly downstream of the symmetry plane containing the two abutments. Given the much larger roughness of the region covered by riprap stone, the highest bed friction velocities are recorded inside the riprap apron. Both the velocity magnitude and the bed friction velocity decay sharply in the recirculation regions forming upstream and downstream of the abutment's lateral faces. This high degree of vertical nonuniformity of the flow is another reason why 2-D numerical models are not expected to be very accurate for flow around abutment placed on the floodplain of a compound channel.

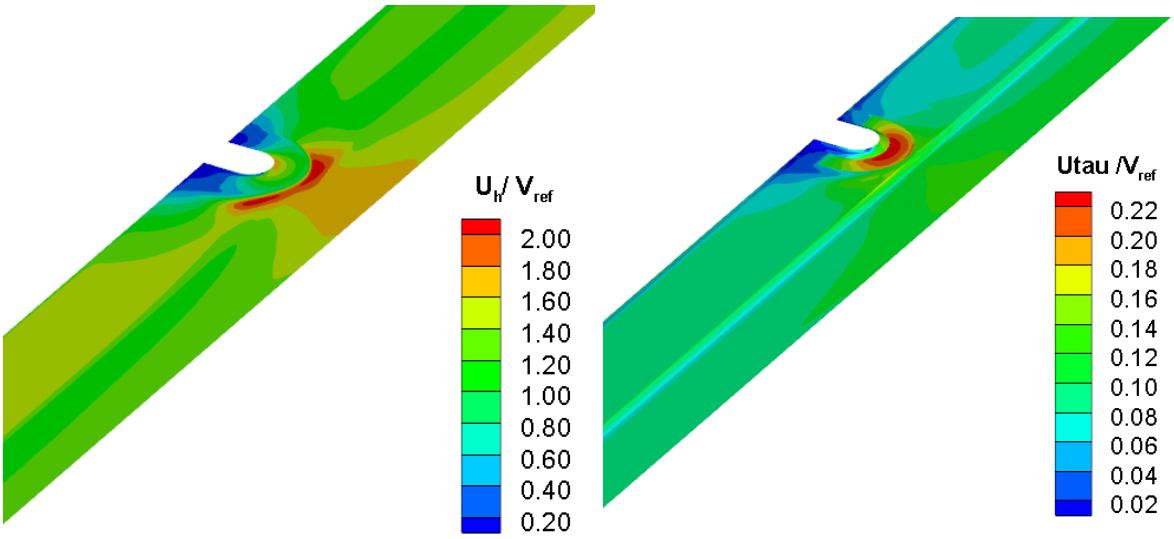

Figure 3.3 Nondimensional free surface velocity magnitude (left) and bed friction velocity over the main channel and its left floodplain (right) for a test case with $D_{50}/H_{ref}=0.4$, $B_f/H_{ref}=14$ and $L_a/H_{ref}=4.9$ (Case III, straight channel). Only half of the domain is shown.

For large channel curvature near the region where the abutments are situated, the flow approaching the abutments is very nonuniform with larger mean velocities developing over the outer side of the channel cross section compared to its inner side (Zeng et al., 2008). This is the main reason why the capacity of the flow to erode the bed near the abutment and its embankments is larger for the outer-bank abutment. This effect is clearly observed by comparing the free-surface velocity magnitude in the L_a/B_f=0.5, D_{50}/H_{ref}=0.2 simulations conducted with R/H_{ref}=∞ (fig. 3.4a) and R/H_{ref}=200 (fig. 3.4b). In these plots the inlet discharges are not equal but the maximum value of the bed shear stress over the riprap region is equal to the treshold value for sediment entrainment. The velocity magnitude of the approach flow is lower in the curved-channel case compared to the straight-channel case, as a lower mean approach flow velocity is needed to induce shear failure of the riprap stone disposed around the toe of the outer-bank abutment. The core of high velocity magnitude inside the main channel moves toward the outer-bank floodplain. The length of the recirculaton region forming behind the outer-bank abutment increases compared to the straight-channel case, while the opposite is true for the recirculation region forming behind the inner-bank abutment (see 2-D streamline patterns in figs. 3.4a and 3.4b). Another interesting observation is that the region of high velocites over the left (outer-bank) floodplain that penetrates to the toe of the abutment in the straight-channel case moves downstream as the channel curvature increases.

For a fixed discharge and B_f, as the abutment length increases, so does the velocity in the contracted flow region. This means for same floodplain width, flow depth, radius of curvature, and median diameter of the riprap stone, the critical bed shear stress value for riprap shear failure is reached for a lower value of the mean incoming velocity in the simulation with a higher L_a/B_f. This can be inferred by comparing the distributions of the velocity magnitude in figure 3.4b

(L_a/B_f=0.5) and figure 3.4c (L_a/B_f=1). The region of maximum free surface velocity magnitude inside the main channel moves downstream and the mean rate of decay away from the peak value is larger in the simulation with a higher L_a/B_f. So, one expects for constant floodplain width, the scour hole inside the main channel will develop at a larger distance away from the toe of each abutment in cases with longer abutments compared to cases with shorter abutments.

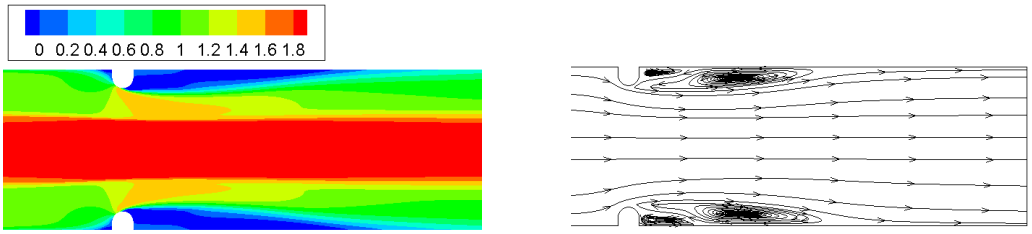

a)

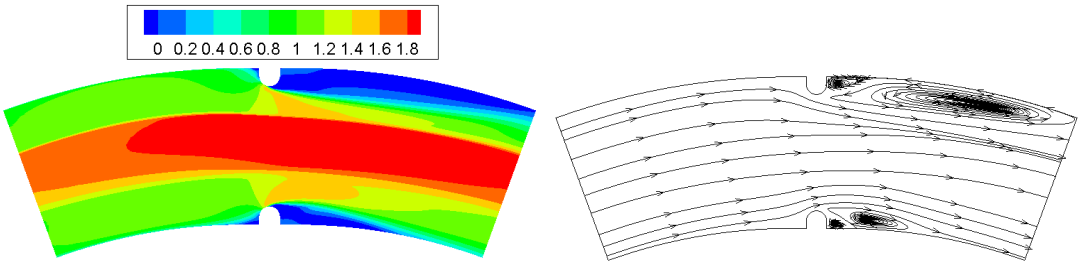

b)

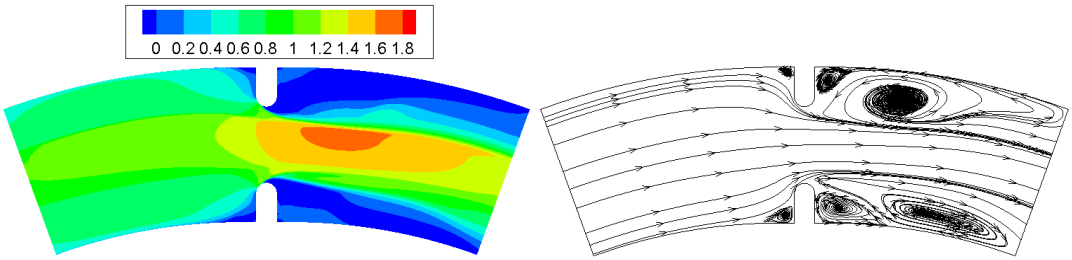

c)

Figure 3.4 Nondimensional streamwise velocity, U_s/V_{ref}, and 2-D streamline patterns at the free surface for Case III (B_f/H_{ref}=14) simulations with D_{50}/H_{ref}=0.2. a) R/H_{ref}=∞ L_a/B_f=0.5; b) R/H_{ref}=200, L_a/B_f=0.5 c) R/H_{ref}=200, L_a/B_f=1.0. Partially reproduced from Wu et al. (2020b).

Figure 3.5 compares the distributions of the nondimensional bed shear stress τ/τ_0 over the outer-bank riprap apron at critical shear failure conditions in several of the Case III simulations conducted with $B_f/H_{ref}=1$. Given that all simulations in figure 3.5 were conducted with $D_{50}/H_{ref}=0.2$, the critical bed shear value is the same ($\tau_c/\tau_0 \approx 3.25$ where $\tau_0=0.0045\rho V_{ref}^2$). In all straight channel simulations with $L_a/B_f \leq 0.7$ the critical bed shear stress at the outer-bank abutment is located next to the toe of the abutment, slightly upstream of its symmetry plane (e.g., see fig. 3.5 for Case III with $L_a/B_f<0.7$). The distribution of τ/τ_0 is qualitatively different in the straight channel simulations with $L_a/B_f=1.0$ where the critical bed shear stress over the riprap apron is situated inside the main channel, close to the end of the transition region between the floodplain and the main channel. For $L_a/B_f=1$ (bottom frame in fig. 3.5), the region of high τ/τ_0 is situated downstream of the abutments' symmetry plane.

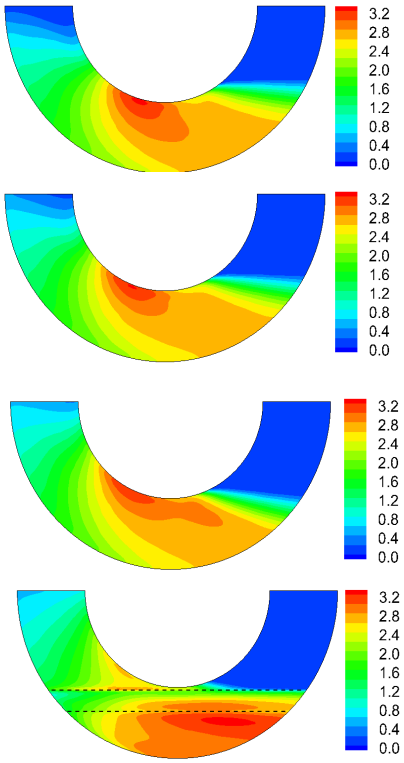

Figure 3.5 Effect relative abutment length (L_a/B_f=0.35, 0.5, 0.7, 1.0) on the nondimensional bed shear stress distribution over the riprap layer at the outer-bank abutment for the straight channel ($R/H_{ref}=\infty$), Case III (B_f/H_{ref}=14) simulations.

Figure 3.6a shows that the main effect of increasing the floodplain width in the straight channel test cases is to move upstream the location of the peak bed shear stress inside the apron. Still, the critical value is recorded in all these cases next to the toe of the abutment.

a)

b)

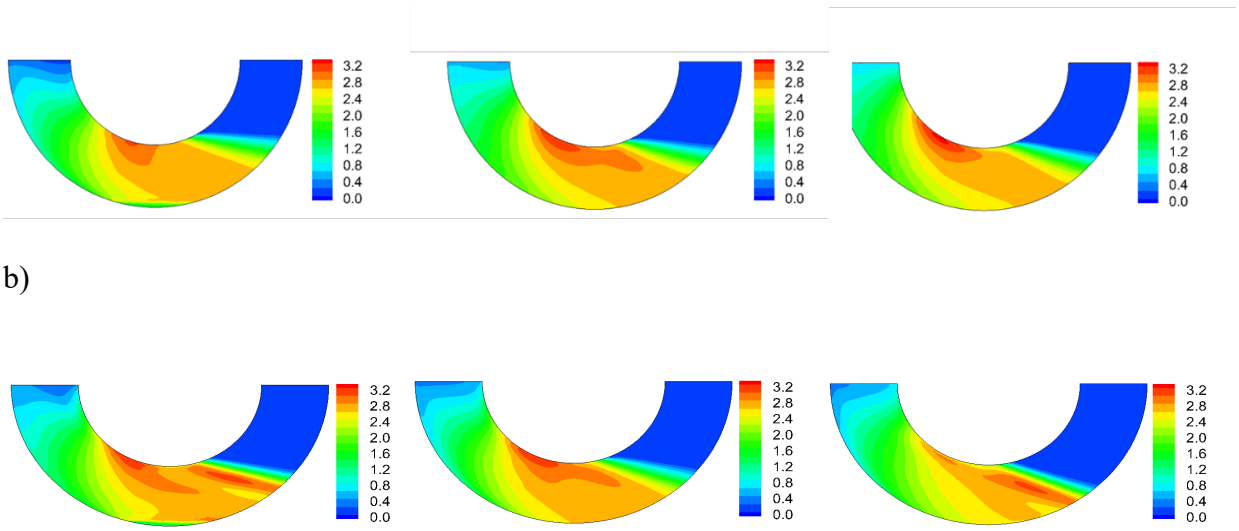

Figure 3.6 Effect of floodplain width (B_f/H_{ref}=10, 14, 30) on the nondimensional bed shear stress distribution over the riprap layer at the outer-bank abutment for simulations conducted with L_a/B_f=0.7. a) straight channel ($R/H_{ref}=\infty$); b) curved channel (R/H_{ref}=200).

Comparison of the corresponding frames in figures 3.6a and 3.6b allows understanding the effect of increasing the channel curvature on the distributions of the bed shear stress inside the riprap apron for cases with $L_a/B_f<1$ where most of the apron is situated over the floodplain. While the peak bed shear stress and the surrounding region of relatively large values of the bed shear stress are situated near the toe of the abutment in the simulations conducted with a straight

channel (e.g., see fig. 3.6a for L_a/B_f=0.7), this is not generally the case as curvature-induced effects become important. As the curvature increases to R/H_{ref}=200 (R/B_m=10), a second region of high bed shear stress forms downstream of the abutment (e.g., see fig. 3.6b for test cases with L_a/B_f=0.7) as the core of high velocities in between the toe of the abutment and the main channel moves downstream. In most of these simulations, the main region of high bed shear stress is situated way downstream of the symmetry plane and has the form of an elongated streak that is situated on the outer side of the shear layer originating at the extremity of the abutment. This effect is partially due to the increase of the width of the region of recirculating flow forming downstream of the outer bank abutment with increasing channel curvature (e.g., compare the 2-D streamline patterns in figs. 3.4a and 3.4b for Case III). The fact that the position of the peak bed shear stress moves away from the toe of the abutment with increasing channel curvature is positive. However, the critical value is reached for a lower discharge with increasing higher channel curvature. So, for the same flooding event (e.g., for the same discharge) it is likely that scour will be more severe at abutments placed in channels with a high curvature near the bridge crossing.

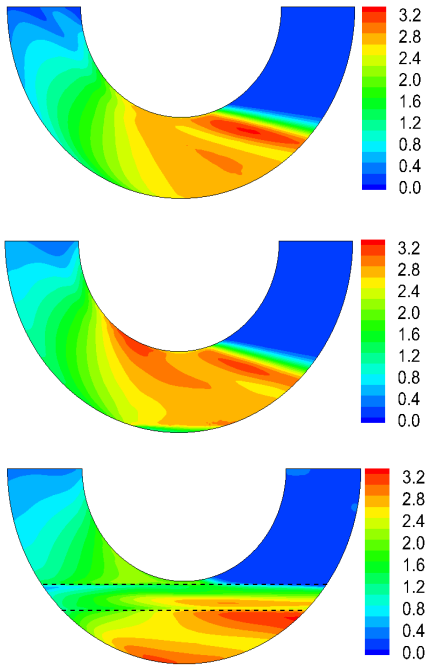

Figure 3.7 Effect relative abutment length (L_a/B_f=0.5, 0.7, 1.0) on the nondimensional bed shear distribution over the riprap layer at the outer-bank abutment for the curved channel (R/H_{ref}=200) Case II (B_f/H_{ref}=10) simulations.

Figure 3.7 allows understanding the effect of increasing the abutment length in the case the abutments are placed in a curved channel with significant curvature effects. For the case when the abutment length is close to equal to the floodplain width, the distributions of the bed shear stress are qualitatively similar, with the highest shear stress over the apron occuring inside the main channel, close to the start of the transition toward the floodplain. In the test cases with $L_a/B_f \leq 0.7$, the main region of high bed shear stress over the apron has a very elongated shape and starts downstream of the symmetry plane containing the centerlines of the two abutments. This region of high bed shear stress corresponds to the one induced by the core of high velocities in between the toe of the abutment and the start of the transition to the main channel. This core of high velocities moves downstream with increasing channel curvature. Thus, for most cases with

relatively high channel curvature, the distribution of the bed shear stress is qualitatively different from that observed in the corresponding straight-channel cases.

3.2 Effect of Relative Abutment Length, Floodplain Width, Channel Radius of Curvature and Riprap Median Diameter on the Critical Froude number

Figure 3.8 summarizes the variation of the critical Froude number ($Fr=V/(gy)^{0.5}$) with D_{50}/y (see Wu et al., 2020b for a more detailed discussion). If $L_a/B_f<1$, the characteristic length scale in the definition of the Froude number is taken as the flow depth over the floodplain, y_f. If $L_a/B_f\approx1$, then y is equal to the flow depth in the main channel, y_m. Also represented in the same figure are the critical Froude number predictions given by the design formulas of Lagasse et al. (2001) and Pagan-Ortiz (1991) proposed for spill-through abutments placed in straight channels. These formulas can be obtained by choosing $K_s=0.89$, $C=0.324$, $\alpha=2.0$ and $K_s=0.535$, $C=0.54$, $\alpha=2.0$ ($Fr<0.8$) in equation 1.1, respectively. An important finding is the Pagan-Ortiz (1991) design formula is not conservative enough for the straight channel test cases (figs. 3.8 and 3.9a). By contrast, Lagasse et al. (2001) formula gives conservative predictions for more than half of the test cases conducted with straight channels (fig. 3.8). These test cases correspond to those for which the floodplain width is fairly small and L_a/B_f is not too high (fig. 3.9a).

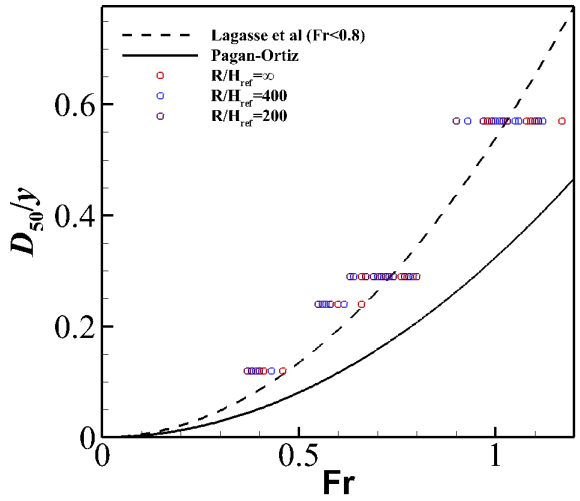

Figure 3.8 Critical Frounde number for spill-wall abutments in compound channels. Also shown are the Lagasse et al. (2001) and Pagán-Ortiz (1991) equations for riprap sizing.

More specifically, figure 3.9a shows that Lagasse et al. (2001) formula provides conservative estimates for all the test cases with B_f/H_{ref}=10 and 14 if $L_a/B_f \leq 0.7$. However, Lagasse et al. (2001) formula is not conservative enough for the test cases with B_f/H_{ref}=20 if L_a/B_f>0.5. For L_a/B_f=1.0, Lagasse et al. (2001) formula provides a conservative estimate only for the test case conducted with the narrowest floodplain width (B_f/H_{ref}=5). Another important finding inferred from figure 3.9 is for both straight and curved channel simulations the critical Froude number decreases monotonically with increasing L_a/B_f for constant flow depth, floodplain width, channel curvature and riprap diameter. This effect is significant and is not taken into account by existing design formulas for spill-through abutments. For example, in the case of an abutment placed in a straight channel with y_m/H_{ref}=1.7, B_f/H_{ref}=20 and D_{50}/H_{ref}=0.2, the critical Froude number decreases from 0.72 to 0.62 as L_a/B_f changes from 0.7 to 0.35 (fig. 3.9a). Moreover, for constant flow depth, channel curvature and riprap median diameter and for abutments extending over the whole width of the floodplain, the effect of increasing the floodplain width is to decrease Fr. For example, for simulations conducted in a straight channel

with y_m/H_{ref}=1.7, L_a/B_f=1 and D_{50}/H_{ref}=0.2, Fr decreases from 0.63 to 0.55 as B_f/H_{ref} increases from 5 to 14 (fig. 3.9a). A similar effect is present in the simulations conducted with R/H_{ref}=400 (fig. 3.9b) and R/H_{ref}=4-200 (Figure 3.9c), though the Froude number range is narrower than the one observed in the corresponding straight channel simulations.

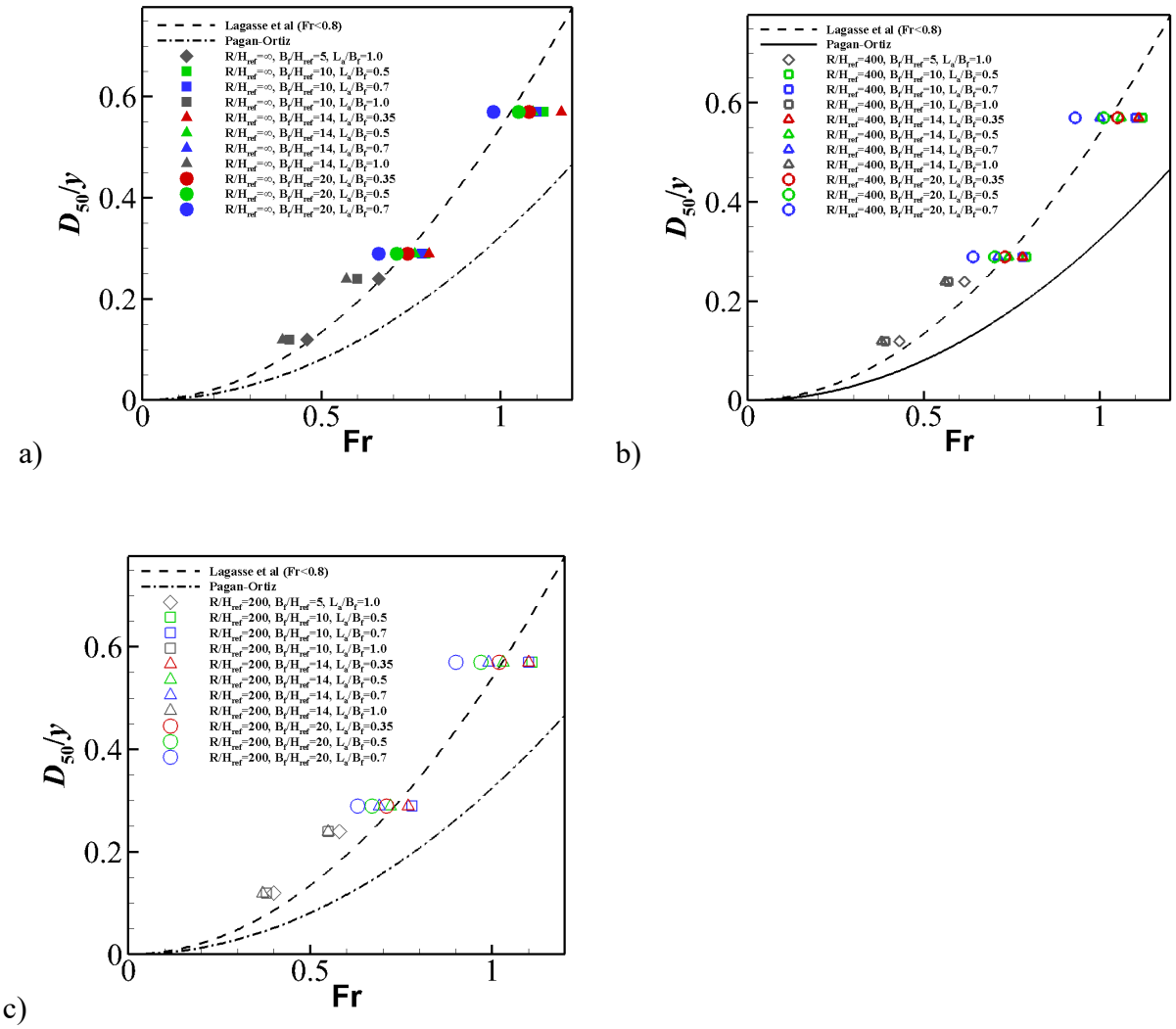

Figure 3.9 Comparison of numerical predictions of the critical Frounde number for spill-wall abutments in channels with: a) R/H_{ref}=∞; b) R/H_{ref}=400; c) R/H_{ref}=200 with Lagasse et al. (2001) and Pagán-Ortiz (1991) equations. Partially reproduced from Wu et al. (2020b).

3.3 Design Formula for Spill-Through Abutments Placed in Straight Channels

The data in figure 3.9a obtained for spill-through abutments placed in a straight channel is used to derive a new riprap sizing formula that retains the functional relationship of equation 1.1. As for the case of wing-wall abutments (Wu et al., 2020a), the model coefficients C and α are expected to be a function of the main geometrical variables defining the compound channel. Additionally, for spill-through abutments one expects the two model coefficients to also be a function of the relative length of the abutment. A main finding is that the parameter α is only function of the floodplain width for test cases with $L_a/B_f<1$ and is independent of L_a/B_f (see also Wu et al., 2020b). This is illustrated in figure 3.10a for the Case II, Case III and Case IV simulations conducted with $L_a/B_f\leq0.7$ for which the variation of D_{50}/y with Fr is linear in log-log scale for each value of L_a/B_f. Moreover, the lines for cases with different values of L_a/B_f are parallel, which means that α assumes the same value for both $L_a/B_f=0.5$ and $L_a/B_f=0.7$. Moreover, the value of α decreases monotonically with increasing floodplain width from $\alpha=1.95$ for $B_f/H_{ref}=10$ to $\alpha=1.75$ for $B_f/H_{ref}=20$. Results also show that the coefficient C is a function of B_f/H_{ref}, L_a/B_f and R/H_{ref}, as shown in table 3.2 that reports the best-fit values for all the straight-channel test cases considered. The coefficient C increases monotonically with L_a/B_f. Also, C increases with increasing floodplain width for constant $L_a/B_f<1$.

Another important finding is that for spill-through abutments with $L_a/B_f=1$, for which the peak bed shear stress over the riprap apron is situated inside of the main channel, α assumes a different value independent of the floodplain width (table 2). This is illustrated in figure 3.10b that shows results for $B_f/H_{ref}=10$ and $L_a/B_f=1$. The variation of D_{50}/y with Fr is linear in log-log scale and the lines are parallel with a slope $\alpha=1.85$.

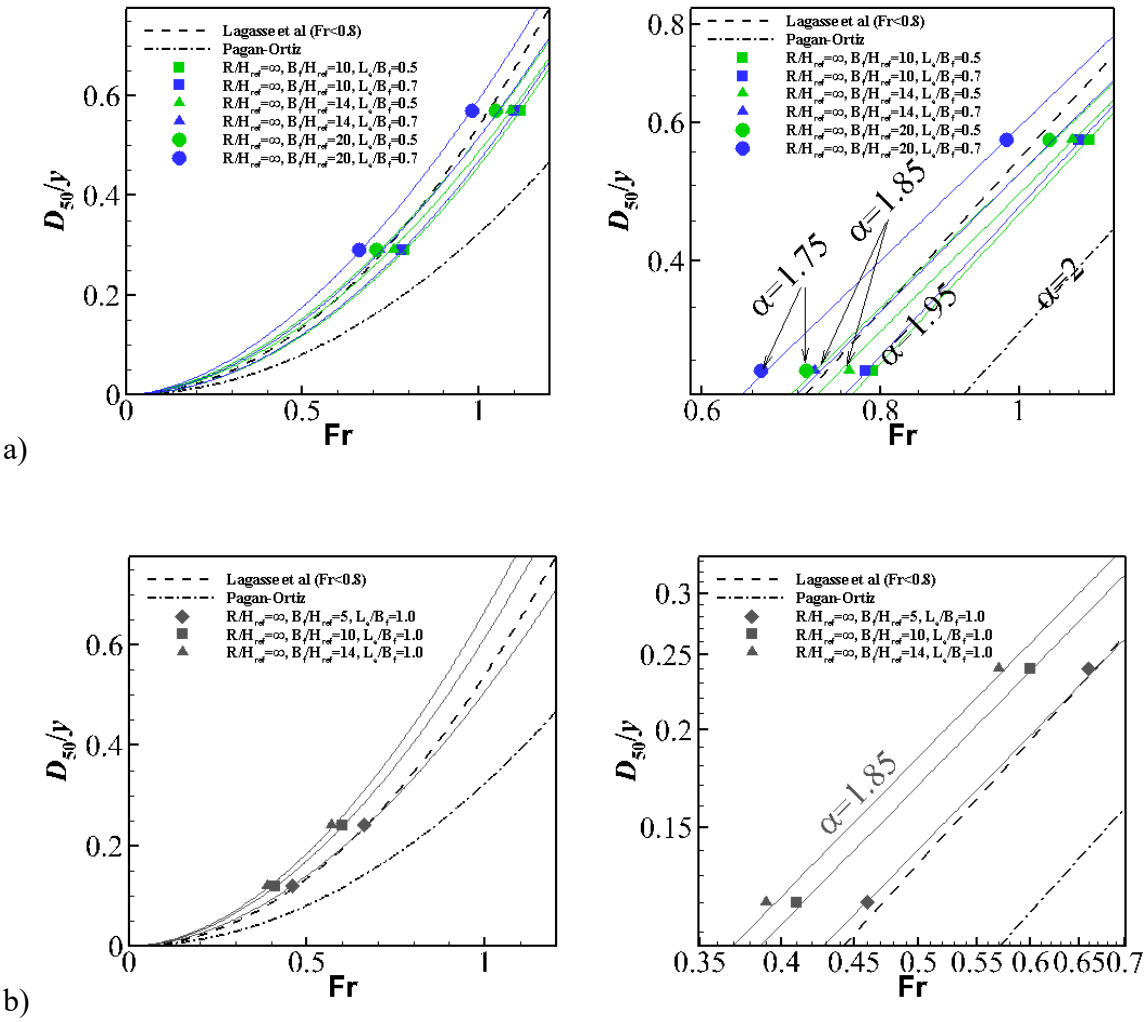

Figure 3.10 Numerical predictions of the critical Froude number for spill-through abutments placed in straight channels. The solid lines show equation (1.1) predictions of the critical Froude number using the α and C values from Table 3.2. a) L_a/B_f=0.5 and 0.7; b) L_a/B_f=1. Results are shown for different values of the floodplain width, B_f/H_{ref}. Also shown are the Lagasse et al. (2001) and Pagán-Ortiz (1991) equations for which α=2.0. The right frames show the same information in log-log scale and serve to estimate the value of α for the simulations with L_a/B_f<1 and L_a/B_f=1.

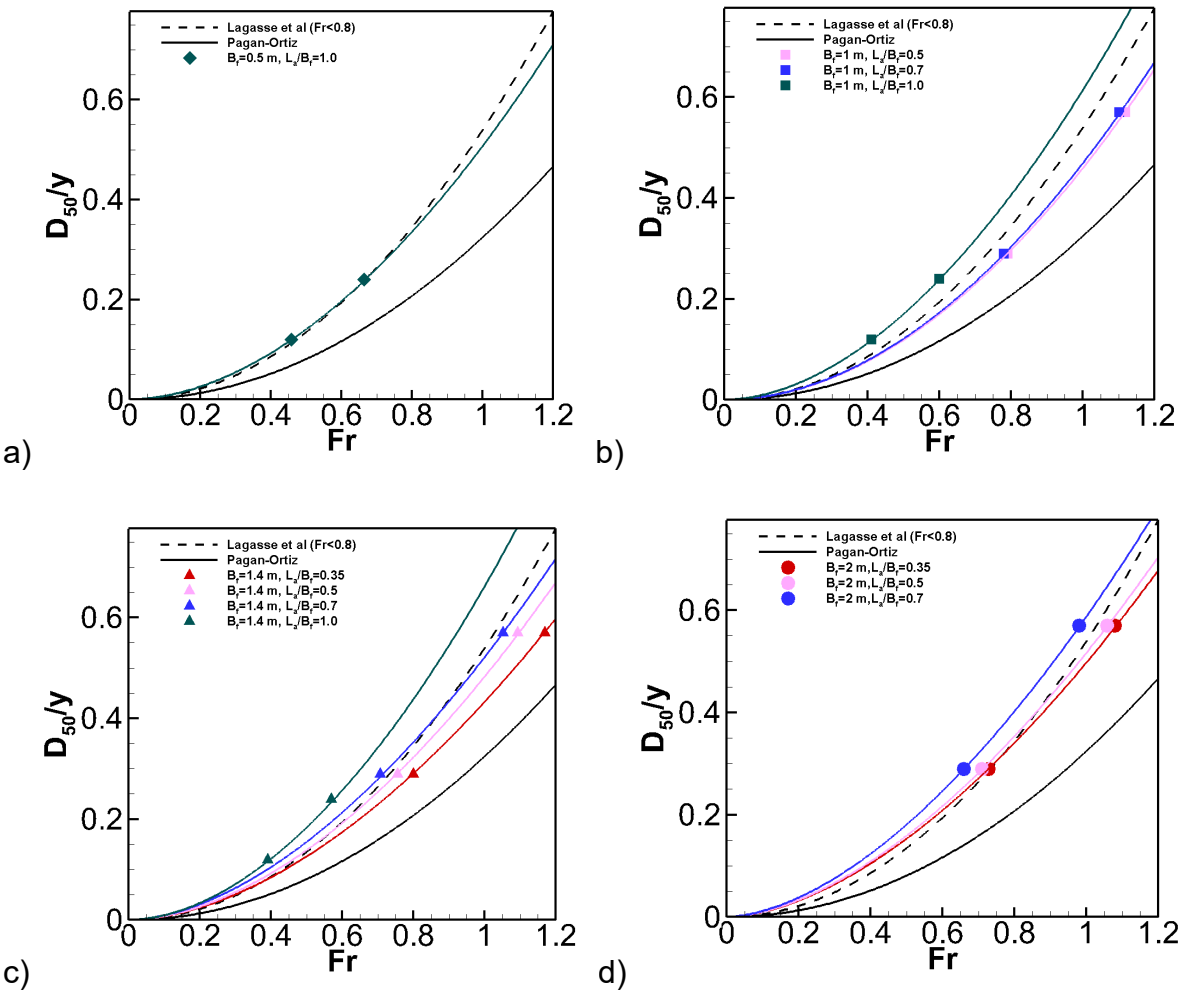

Figure 3.11 Comparison between the numerical predictions of the critical Froude number and Lagasse et al. (2001) and Pagán-Ortiz (1991) equations for spill-through abutments placed in a straight compound channel. a) B_f/H_{ref}=5; b) B_f/H_{ref}=10; c) B_f/H_{ref} =14; d) B_f/H_{ref} =20. The colored lines show equation (1.1) predictions of the critical Froude number using the α and C values from table 3.2.

As shown in figure 3.11, the design formula predictions of the critical Froude number are close to the data determined from numerical simulations for all the test cases conducted with $L_a/B_f \leq 1$ and $B_f/H_{ref} \leq 20$. For constant $L_a/B_f < 1$, the Froude number decreases with increasing floodplain width (Figure 3.12 and Table 3.2).

Table 3.2 Best fit values of the power coefficient α and of the coefficient C as a function of the nondimensional abutment length L_a/B_f and floodplain width, B_f/H_{ref}.

	Case I B_f/H_{ref}=5	Case II B_f/H_{ref}=10	Case III B_f/H_{ref}=14	Case IV B_f/H_{ref}=20	Case IV B_f/H_{ref}=20 (SBR)
L_a/B_f=0.35			α=1.80 C=0.39	α=1.75 C=0.45	α=1.75 C=0.75
L_a/B_f=0.5		α=1.95 C=0.45	α=1.80 C=0.45	α=1.75 C=0.47	α=1.75 C=0.76
L_a/B_f=0.7		α=1.95 C=0.46	α=1.80 C=0.48	α=1.75 C=0.55	α=1.75 C=0.77
L_a/B_f=1.0	α=1.85 C=0.48	α=1.85 C=0.59	α=1.85 C=0.64		

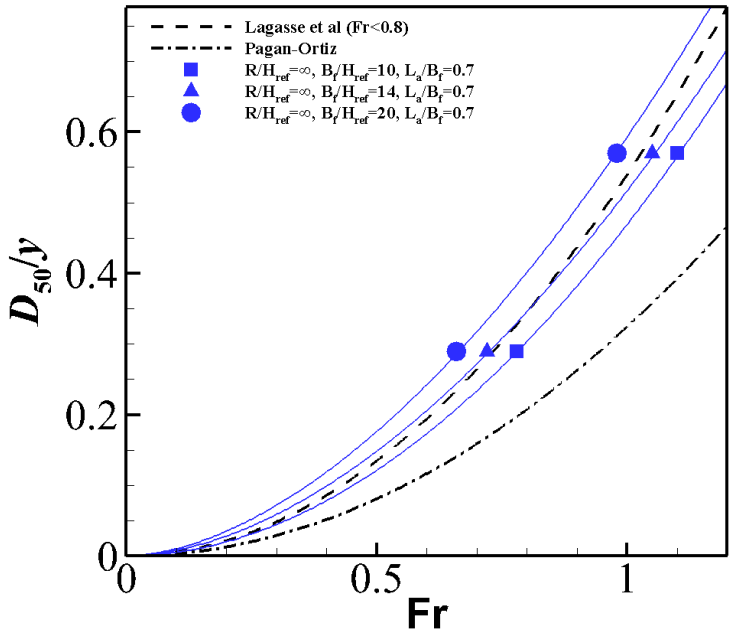

Figure 3.12 Critical Froude number as a function of floodplain width, B_f/H_{ref}, and riprap size, D_{50}/y_m, for the simulations conducted with spill-through abutments with L_a/B_f=0.7. The solid lines show equation (1.1) predictions of the critical Froude number using the α and C values from table 3.2.

Figure 3.13 shows the critical Froude number for the simulations conducted with B_f/H_{ref}=20 and L_a/B_f=0.35, 0.5, 0.7. These plots contain two set of curves and symbols. The circle symbols correspond to the critical Froude number being calculated with the mean velocity in the contracted section between the two abutments and with the flow depth over the floodplain. These predictions are relatively close to those given by Lagasse et al. (2001) equation, though the Lagasse et al. (2001) formula underestimates the critical Froude number for most of the test cases with L_a/B_f=0.5 and for all test cases with L_a/B_f=0.7. For test cases with a relatively small length of the abutment, HEC-23 (Lagasse et al., 2009) recommends using a different velocity scale equal to the mean velocity over the floodplain containing each abutment in the contracted, bridge opening section. The recommended switch from using the mean velocity in the full contracted section to using the mean velocity over the floodplain is when the set-back ratio (SBR) is larger than 5, where SBR is the ratio of the set-back length for the abutment, B_f-L_a, to the average flow depth in the channel. This switch in the definition of the velocity scale is physically sound, though the threshold value SBR=5 is somewhat arbitrary. Only Case IV test cases are good candidates for using the SBR method as SBR=3.5 for L_a/B_f=0.7 and SBR≥6.0 for the lower L_a/B_f values.

The triangle symbols in figure 3.13 correspond to critical Froude number estimations using the SBR method. As the mean velocity over the floodplain containing the abutment is less than the mean velocity in the contracted section, the critical Froude number calculated using the corrected velocity scale is less than the one calculated using the standard definition. The same procedure can be used to calculate the two parameters in the new design formula. The design equation curves approximate the data when the new velocity scale is used. Interestingly, the value of the coefficient α estimated using the new velocity scale remains the same for all Case

IV simulations (α=1.75, see Table 3.2). As for calculations performed using the standard velocity scale, the coefficient C increases monotonically with L_a/B_f for constant channel curvature and floodplain width.

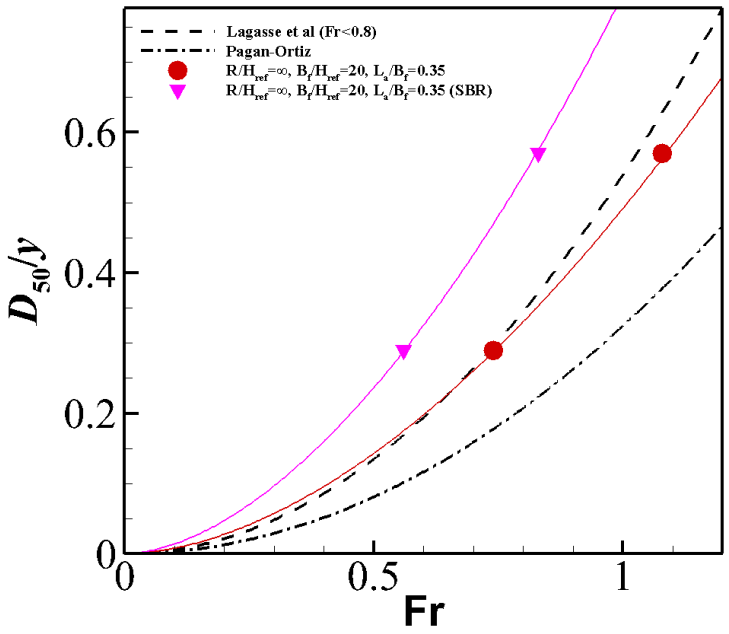

a)

b)

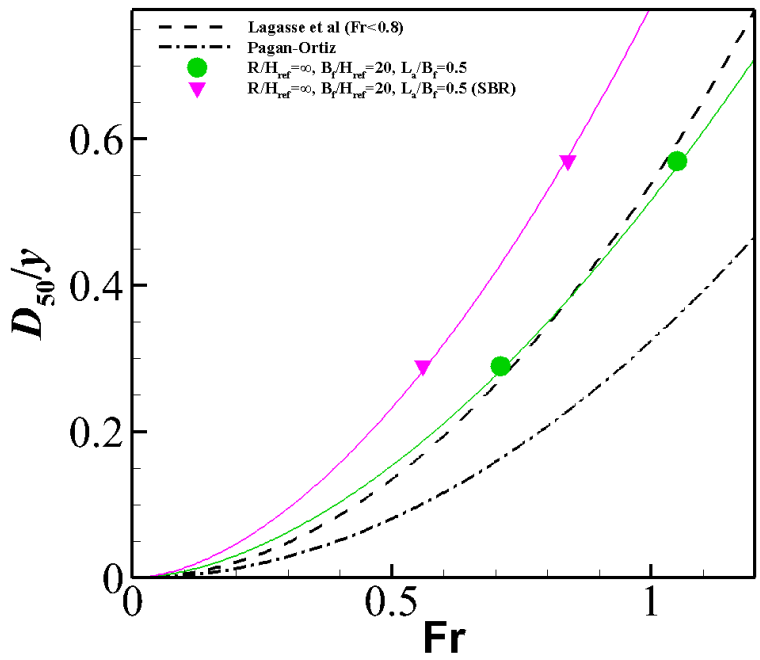

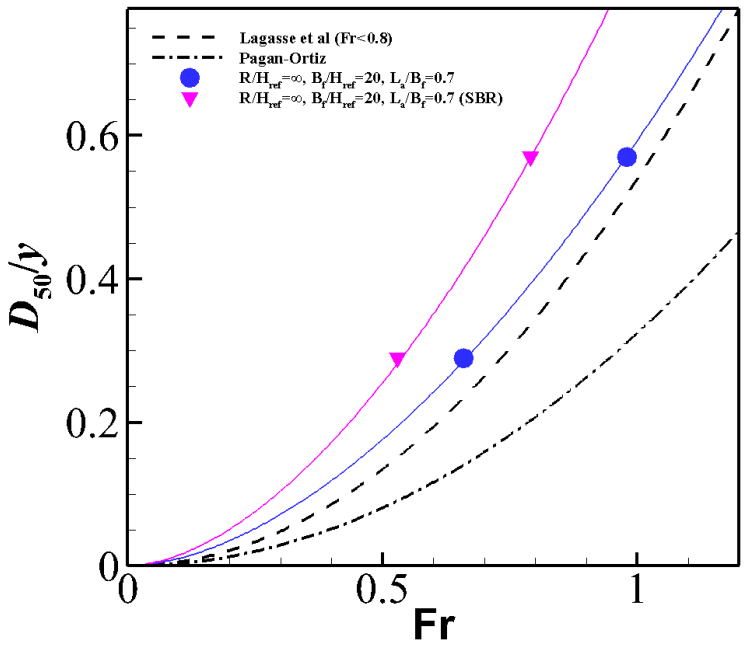

c)

Figure 3.13 Critical Froude number as a function of relative abutment length L_a/B_f, and riprap size, D_{50}/y_m, for the Case IV simulations conducted with B_f/H_{ref}=20. a) L_a/B_f=0.35; b) L_a/B_f=0.5; c) L_a/B_f=0.7. Results are shown with the Froude number calculated using the standard method (circles) and the SBR method (triangles). The solid lines show equation (1.1) predictions of the critical Froude number using α=1.75 and the C values from table 3.2. Also shown are the Lagasse et al. (2001) and Pagán-Ortiz (1991) equations for which α=2.0.

Chapter 4 Conclusions and Proposed Future Work

As part of the present research project, a general methodology based on fully 3-D, non-hydrostatic RANS numerical simulations was developed to determine the conditions for riprap shear failure for cases when a riprap apron is placed close to an abutment in a compound channel. The relationship proposed by Melville and Coleman (2000) and Melville et al. (2007) for riprap entrainment threshold (shear failure mode) was used to determine if riprap stone entrainment occurs. The methodology was validated during Year 1 for wing-wall abutments using the experimental data of Melville et al. (2007). Based on data obtained using this methodology, a new riprap sizing design formula was proposed for wing-wall abutments in Year 2. The proposed numerical approach is much less expensive compared to the classical one based on laboratory scaled-model investigations and allows incorporating additional complexities present at many bridge sites in the field.

A main finding of the study carried during Year 3 for spill-through abutments placed in a compound straight channel was the data generated via numerical simulations showed Lagasse et al. (2001) formula gave more accurate predictions compared to Pagan-Ortiz (1991) formula. Still, even Lagasse et al. (2001) formula overpredicted the critical value of the Froude number for test cases conducted with high values of the floodplain width (e.g., B_f=2.0 m). Slight overpredictions were observed even for smaller values of B_f if the relative length of the abutment, L_a/B_f, was sufficiently large. The critical Froude number was found to decay monotonically with the decrease in L_a/B_f, an effect not accounted for in any existing design formulas.

The main outcome of the research performed during Year 3 was to propose a new two-parameter, riprap sizing formula for protection of spill-through abutments against erosion. The

formula can be used for cases when the channel curvature is negligible in the region where the abutments are situated. The formula incorporates the effects of some of the main geometrical variables (floodplain width, relative abutment length) on the minimum median diameter of the rock riprap, D_{50}, that will resist shear failure. The formula retains the functional relationship ($D_{50}/y=C^{0.5\alpha}*Fr^{\alpha}$) of Lagasse et al. (2001) and Pagan-Ortiz (1999) formulas used for riprap apron design at abutments.

Though, in principle, the two model parameters C and α should be a function of the main nondimensional geometrical parameters (e.g., L_a/B_f, B_f), analysis of the data showed that α is only a function of the floodplain width for cases where the abutment length is not very close to the floodplain width. In the latter cases, the apron extends into the main channel and the maximum bed shear stress over the apron is situated inside the main channel rather than the floodplain. The predicted values of α ($1.75<\alpha<1.95$) for the test cases with $L_a/B_f<1$ were slightly lower than the value ($\alpha=2$) used in the design formulas of Lagasse et al. (2001) and Pagan-Ortiz (1991). Moreover, α was found to decay monotonically with increasing floodplain width. For cases with $L_a/B_f=1$, the best fit to the data predicted $\alpha=1.85$ independent of the floodplain width. The new design formula was found to fit all data generated via numerical simulations conducted in compound channels containing spill-through abutments with varying B_f and L_a/B_f.

During Year 4, the data obtained for spill-through abutments placed in curved compound channels will be used to extend the proposed riprap sizing formula for bridges positioned in regions where bank-curvature effects are important. The other main objective of Year 4 will be to generate data and propose a design formula for cases when the flow regime beneath the bridge deck connecting the two abutments changes from free surface flow to orifice flow or to fully-

pressurized flow. Such a regime change induces very complex changes in the velocity and bed shear stress distribution inside the pressurized-flow region and downstream of it.

We will work with the Transportation Research Board committee TRB-AFB60 such that the main findings and the proposed new design formulas for determining minimum riprap size at wing-wall and spill-through abutments will be considered for adoption in a future FHWA Technical Brief update to HEC 23. Once adopted, the new procedure will enhance the capabilities of state DOTs to develop more reliable approaches to protect bridges against possible failure induced by severe erosion associated with flood events. At a more general level, more accurate riprap design formulas for protection of abutments against erosion will result in significant reduction of the costs to operate roads during and after flood events. It will also contribute to reducing the risk for hazards associated with bridge failure during floods by avoiding structural failure.

References

Barkdoll, B. D., Ettema, R., & Melville, B. W. (2007). *Countermeasures to protect bridge abutments from scour* (NCHRP Project 24-18. NCHRP Report 587). Transportation Research Board.

Brown, S. A., & Clyde, E. S. (1989). *Design of riprap revetment: Hydraulic Engineering Circular No. 11* (FHWA-IP-016). National Highway Institute (US).

Cardoso, A., Simarro, G. and Schleiss, A. (2010). *Sizing of riprap for spill-through abutments, Water Management*, 163, issue WM10, 499-507, Paper 900024.

Cheng, Z., Koken, M. and Constantinescu, G. (2018). Approximate methodology to account for effects of coherent structures on sediment entrainment in RANS simulations with a movable bed and applications to pier scour. *Advances in Water Resources,* 120, 65-82

Chiew, Y. M. (1995). Mechanics of riprap failure at bridge piers. *Journal of Hydraulic Engineering*, *121*(9), 635-643.

Dey, S. & Barbhuiya, A.K. (2005). Time variation of scour at abutments. *Journal of Hydraulic Engineering, 131(1),* 11-23.

Ettema, R, Constantinescu, G and Melville, B. (2011). *NCHRP 24-27(01): Evaluation of bridge pier scour research: scour processes and estimation*. Final report for NCHRP.

Ettema, R., Ng, K., Chakradhar, R., Fuller, J., & Kempema, E. W. (2015). Failure of spill-through bridge abutments during scour: Flume and field observations. *Journal of Hydraulic Engineering, 141(5),* 06015001.

Ettema, R., Constantinescu, G., & Melville, B. W. (2017). Flow-field complexity and design estimation of pier-scour depth: Sixty years since Laursen and Toch. *Journal of Hydraulics Engineering*, *143*(9), 03117006.

Hoffmans, G. J., & Verheij, H. J. (1997). *Scour manual* (Vol. 96). A.A. Balkema, Rotterdam, Netherlands.

Hong, S. H., and Abid, I. (2019). Scour around an erodible abutment with riprap apron over time. *Journal of Hydraulic Engineering, 145(6),* 06019007

Horna-Munoz, D. and Constantinescu, G. (2018). A fully 3-D numerical model to predict flood wave propagation and assess efficiency of flood protection measures. *Advances in Water Resources, 122*, 148-165

Horna-Munoz, D. and Constantinescu, G. (2020) 3-D dam break flow simulations in simplified and complex domains, *Advances in Water Resources*, *137*, 103510, https://doi.org/10.1016/j.advwatres.2020.103510.

Koken, M., & Constantinescu, G. (2014). Flow and turbulence structure around abutments with sloped sidewalls. *Journal of Hydraulic Engineering*, *140*(7). 04014031.

Kothyari, U.C., Hager, W.H. and Oliveto, G. (2007). Generalized approach for clearwater scour at bridge foundation elements, *Journal Hydraulic Engineering, 133(11),* 1229-1240.

Lagasse, P, Zevenberger,L., Schall, J and Chopper, P. (2001). *Bridge scour and stream instability countermeasures: experience, selection, and design guidance: Hydraulic Engineering Circular No. 23* (FHWA-NH1-01-003). National Highway Institute (US).

Lagasse, P. F., Clopper, P. E., Pagán-Ortiz, J. E., Zevenbergen, L. W., Arneson, L. A., Schall, J. D., & Girard, L. G. (2009). *Bridge scour and stream instability countermeasures: experience, selection, and design guidance: Hydraulic Engineering Circular No. 23* (FHWA-NHI-09-111). National Highway Institute (US).

Melville, B. W. and Coleman, S. E. (2000). *Bridge scour.* Water Resources Publications, Littleton, Colorado.

Melville, B., van Ballegooy, S., Coleman, S. and Barkdoll, B. (2006a). Countermeasures to protection at spill-through abutments. *Journal of Hydraulic Engineering*, *132*:235-245.

Melville, B., van Ballegooy, S., Coleman, S. and Barkdoll, B. (2006b). Scour countermeasures for wing wall abutments. *Journal of Hydraulic Engineering, 132*:563-574.

Melville, B., Van Ballegooy, S., Coleman, S. and Barkdoll, B. (2007). Riprap selection at wing wall abutments. *Journal of Hydraulic Engineering,133*:1265-1269.

NCHRP Project 24-18 (*NCHRP Report 587*), *Countermeasures to Protect Bridge Abutments from Scour.*

NCHRP Project 24-19, *Selection Criteria and Design Guidelines, and techniques for the Size and Placement of Environmentally Sensitive Channel and Bank Protection Measures, and Quality Control*.

NCHRP Project 24-20, *Prediction of Scour at Bridge Abutments*.

Pagaz-Ortiz, J. (1991). *Stability of rock riprap for protection at the toe of abutments located at the flood plain, Rep. No. FHWA-Rd-91-057*, Federal Highway Administration, US Dept. of Transportation, Washington, DC.

Roulund, A., Sumer, M., Fredsoe, J. ad Michelsen, J. (2005). Numerical and experimental investigations of flow and scour around a circular pile. *Journal of Fluid Mechanics, 534,* 351-401.

Sturm, T. W., & Janjua, N. S. (1994). Clear water scour around abutments in floodplains. *Journal of Hydraulic Engineering*, *120*(8), 956-972.

Sturm, T. W., Ettema, R., & Melville, B. W. (2011). *Evaluation of bridge-scour research: Abutment and contraction scour processes and prediction (pp. 24-27).* Washington, DC, USA: National Cooperative Highway Research Program, Transportation Research Board of the National Academies.

Sumer, B. M. and Fredsoe J. (2002). *The mechanics of scour in the marine environment*. World Scientific.

Wu, H., Zeng, J. and Constantinescu, G. (2020a). A multi-parameter design formula for riprap size selection at wing-wall abutments, *Journal Hydraulic Research*, paper TJHR-2019-0218, https://doi.org/10.1080/00221686.2020.1818310

Wu, H., Zeng, J. and Constantinescu, G. (2020b). A design formula for sizing rock riprap at spill-through abutments in compund channels, *Journal Hydraulic Engineering*, under review

Zeng, J., Constantinescu, G., Blanckaert, K., & Weber, L. (2008). Flow and bathymetry in sharp open-channel bends: Experiments and predictions. *Water Resources Research*, *44*(9), W09401.